Hallis et al. (2025)
The D/H ratio of the Martian Mantle: Evidence from the Lafayette Meteorite
Advances in Geochemistry and Cosmochemistry 1(2): 761, https://doi.org/10.33063/agc.v1i2.761

Research article

The D/H ratio of the Martian Mantle: Evidence from the Lafayette Meteorite

Lydia J. Hallis[1,2]✉ Evangelos Christou[1] Jemma Davidson[3] Andrea G. Distel[3] Richard L. Hervig[3]

[1] School of Geographical and Earth Sciences, University of Glasgow, Molema Building, Lillybank Gardens G12 8QQ, UK
[2] The Natural History Museum London, Cromwell Road, South Kensington, London SW7 5BD
[3] School of Earth and Space Exploration, Arizona State University, 781 East Terrace Road, Tempe, AZ 85287-6004, USA

✉ **Correspondence to:** L.J. Hallis: Lydia.hallis@glasgow.ac.uk

Author contributions: Conceptualization: LJH; Data curation: LJH, JD, AGD, RLH; Funding acquisition: LJH, EC; Investigation: EC; Methodology: JD, AGD, RLH; Writing – original draft: LJH; Writing – review & editing: JD, AGD, RLH.

Data, code, and outputs: http://doi.org/10.60520/IEDA/113748

Submitted: 2025-04-24
Accepted: 2025-11-08
Published: 2025-12-19

Production editor: Ananya Mallik

Handling editor: Romain Tartèse

Reviews: Two anonymous reviewers

Copyediting: Anselm Loges, Marthe Klöcking

Hydrous apatite in the nakhlite group of martian meteorites shows evidence of Cl-rich fluid incorporation into the magma prior to apatite crystallisation. Thus, nakhlite apatite D/H ratios should reflect a mixture between the parental magma and this crustally derived fluid. Here we present the volatile content and D/H ratios of apatite within the nakhlite Lafayette (δD 137 to 352 ‰), suggesting mixing between a crustally derived Cl-rich fluid and an intermediate D/H ratio (δD ≈ 400 ‰) and a magma with a low D/H ratio (δD ≈ −100 ‰). This martian mantle D/H ratio is similar to that of Earth's upper mantle, but is higher than recent D/H ratios measured within a number of other inner Solar System materials. Thus, D/H ratio heterogeneity in these materials points towards multiple sources of hydrogen during the formation of rocky planetary bodies in the inner Solar System.

1 Introduction

Mars has lost a large proportion of its atmosphere to space over time, with the surface environment becoming colder and drier (e.g., Jakosky et al., 2018; Dong et al., 2018; Jakosky and Hallis, 2024). This atmospheric loss has driven isotopic fractionation, with the lighter isotopes of volatile elements being preferentially lost (e.g., Webster et al., 2013). In particular, this effect is observed in the extreme for hydrogen isotopes (e.g., Villanueva et al., 2015), where the lighter isotope (^{1}H) is half the mass of the heavier isotope (^{2}H or D). This fractionation poses a problem for defining the original hydrogen isotope (D/H) ratio of Mars – an important factor in determining the building blocks during Mars' formation. In order to determine the original hydrogen isotope (D/H) ratio of the martian mantle, a source region unaffected by the atmospheric loss must be measured.

Ahead of Mars Sample Return (MSR), martian meteorites are the only samples of Mars available for study here on Earth. As such, they can provide vital information about the composition and evolution of the martian atmosphere, crust and mantle, albeit at limited times and places (Udry et al., 2025). Several groups of largely basaltic igneous meteorites are currently known, divided according to their crystallisation age and petrogenesis on Mars (e.g., Udry et al., 2020). Of these groups, the nakhlites contain some of the least shocked and least terrestrially contaminated meteorites (e.g., Treiman, 2005), thus some of the most promising samples for the study of martian volatile elements.

The nakhlite group (22 individual meteorites, with some pairings) are all sourced from a single site on Mars, emplaced as multiple basaltic lava flows and/or sub-surface intrusions at ≈ 1.3 Ga (e.g., Nyquist et al., 2001; Okazaki et al., 2003; Treiman, 2005; Misawa et al., 2005; Cohen et al., 2017; Udry and Day, 2018; Daly et al., 2019b; Udry et al., 2020). The nakhlites are olivine-bearing clinopyroxenites with a fine-grained mesostasis, indicative of slow phenocryst growth within a sub-surface magma chamber, followed by a faster cooling stage upon extrusion to the surface/near-surface (Lentz et al., 1999; Day et al., 2006; Udry and Day, 2018; Daly et al., 2019b). Based on bulk-rock major and trace element concentrations there appear to be two sub-groups of nakhlites: those with higher trace element abundances and lower MgO contents, and those with lower trace element

abundances and higher MgO contents (Udry and Day, 2018). These sub-groups are also evident via variations in mean modal mineral abundances and abundance ranges of pyroxene, olivine, and mesostasis. The higher trace element lower MgO group (e.g., the Miller Range nakhlites and Northwest Africa 5790) is characterised by low modal olivine and pyroxene-mesostasis covariance, whereas the lower trace element higher MgO group (including Lafayette, Nakhla, Governador Valadares, and the Yamato nakhlite pairing group) is characterised by low modal mesostasis and pyroxene-olivine covariance (Corrigan et al., 2015).

Apatite, $Ca_5(PO_4)_3(F, Cl, OH)$, is present as a minor mineral within the nakhlites, forming at a late stage in the crystallisation sequence, thus typically located within the mesostasis as small crystals (commonly 5–50 µm diameter). Despite its small and rare nature, apatite has been heavily studied in the nakhlites because of its volatile-rich composition. The variation in F, Cl, and OH abundance within nakhlite apatite suggests that a Cl-enriched exogenous fluid was incorporated into the magma prior to apatite crystallisation (McCubbin et al., 2013; Birski et al., 2019). This theory is supported by apatite F, Cl, and OH abundances (McCubbin and Nekvasil, 2008) as well as Cl isotope data (Shearer et al., 2018), from the chassignite martian meteorites, a group that are petrogenetically related to the nakhlites. This fluid is reported to have a martian crustal origin – either added to the nakhlite magma via mixing with magma containing an assimilated crustal component (Treiman, 2005) or via the direct addition of a Cl-rich crustal fluid or sediment (McCubbin and Nekvasil, 2008; McCubbin et al., 2013; Martínez et al., 2023). In either case it follows that the hydrogen within nakhlite apatite should have a D/H isotope ratio representing a mixture between the parental magma and the crustal component at the nakhlite launch site. Note that hydrogen isotopes are not significantly fractionated during partial melting or crystallization, although they can be affected by degassing (e.g., Tartèse et al., 2014; Peslier et al., 2019). The D/H ratio of nakhlite apatite has been previously reported. Apatite crystals within the Nakhla meteorite contain low D/H ratios ($\delta D \approx -78$–188 ‰; Hallis et al., 2012). However, these analyses are limited to three apatite crystals in a single meteorite. To augment this dataset we present the volatile content and D/H ratios of apatite within the Lafayette meteorite, a minimally terrestrially altered nakhlite from the low trace-element high MgO sub-group (similar to Nakhla; Udry and Day, 2018; O'Brien et al., 2022).

2 Methods

2.1 Imaging via scanning electron microscopy

Lafayette thin-section SM-505 was loaned for this research by the Smithsonian Institution National Museum of Natural History, Wahington D.C., USA. Apatite grains were located within this thin-section, and an overview of the section's mineralogy was gained via scanning electron microscopy (SEM) backscatter electron (BSE) imaging and energy dispersive X-ray spectrometry (EDS). The University of Glasgow Sigma variable pressure field emission SEM housed within the School of Geographical and Earth Sciences GEMS facility was utilised for these analyses (probe current of 2 nA, accelerating voltage of 20 kV and working distance of 8.5 mm), as well as the London Natural History Museum (NHM) Zeiss Ultra plus SEM equipped with an AZtec EDS system and a ULTIM Max 170 EDS detector (probe current of 1.3 nA, accelerating voltage of 20 kV). A 10 nm carbon coating was added to the thin-section prior to SEM analyses. Cathodoluminescence images were produced of several apatite grains using the NHM Zeiss evo-15LS GATAN Chroma colour CL system, with a 15 kV accelerating voltage, a 3 nA probe current, and a 5 ms dwell time.

2.2 Quantitative mineral chemical analyses

Apatite major and minor element chemistries were determined via electron microprobe analyses (EMPA) using the University of Edinburgh Cameca SX100 housed within the School of Geosciences. The analytical conditions of the electron microprobe included a 100 nA primary beam current, 15 kV accelerating voltage, and 2 µm spot size. The primary beam current for beam-sensitive elements (e.g., Na, F, P, and Ca) was set at 4 nA. Beam-sensitive elements were measured first. Matrix effects were corrected using PAP procedures. The following reference materials were used: Apatite P K4 for P, Ca and F; Jadeite-BL7 for Na; Spinel-BL8 for Mg and Al; Wollastonite-BL7 for Si; NaCl-BLOwn for Cl; Barite-BL7 for S, Orthoclase-BL7 for K; PuMn-BL8 for Mn; Fayalite for Fe; Rutile-BL8 for Ti; PuCr-BL8 for Cr.

Based on 13 anions, stoichiometric calculations were made to determine the ratio of Cl:F:OH in the apatite X-site. Although OH cannot be directly detected via EMPA, its abundance can be calculated based on the assumption that only Cl, F, and OH are present in the X-site (see McCubbin et al., 2013, for details).

Note that our EMPA measurements were completed before SIMS analyses, in order to allow the measurement of the same area for major and minor elements and D/H ratios. In addition, EMPA had to be completed prior to SIMS analyses as the apatite grains were too small to allow EMPA analyses after the production of a SIMS pit. However, Barnes et al. (2013) showed that H mobilisation during EMPA analyses is not an issue, and that lunar apatite D/H ratios were not altered by EMPA.

2.3 Hydrogen isotope analyses

Apatite hydrogen isotope ratios and water abundances were determined using the Cameca IMS 6f secondary ion mass spectrometer (SIMS) at Arizona State University, using analytical protocols similar to those described in Davidson et al. (2020). The instrument was baked prior to the analytical session for 68 hours followed by ≈18 hours of Ti-sublimation pump use to improve the vacuum and reduce the inherent H background, producing a vacuum within the analysis chamber of 2.5–3.6×10^{-10} Torr (3.3–4.8×10^{-8} Pa). The Ti-sublimation pump was also used

each night throughout the analytical sessions to maintain the low H background. The H_2O background within the analytical chamber averaged ≈7 µg/g, measured via the analysis of a San Carlos olivine standard (< 1 µg/g water; Mosenfelder et al., 2011; Harries et al., 2023). For further details on background calculations, plus IMF values and corrections on individual measurements see Supplementary Material and Hallis et al. (2025). An electron gun was employed to maintain charge balance and measurements were undertaken with a Cs^+ primary beam at 2 nA for unknown apatite and 20 nA for reference materials and nominally anhydrous minerals (e.g., augite). The beam was rastered over a ≈30 µm × 30 µm area. A 10-minute, ≈60 µm × 60 µm pre-sputter at the same primary beam conditions was also used for each analysis. A field aperture was used to limit the analysed area to a circular ≈15 µm diameter area centred on the rastered region, reducing background H counts associated with crater edges. Each measurement consisted of up to 50 consecutive cycles each of H^-, D^-, and $^{16}O^-$ with counting times of 1 s, 10 s, and 1 s, respectively. The H_2O concentrations were estimated via a $H^-/^{16}O^-$ vs. H_2O calibration curve based on data from Durango and Crystal Lode reference apatite crystals, as well as the anhydrous San Carlos olivine reference, mounted together in indium and coated with 20 nm carbon. Water content calibrations were performed via the method of Mosenfelder et al. (2011), see Supplementary Material.

Hydrogen isotopic ratios (the ratio of ^2H or D to ^1H) are reported as deviations from Vienna Standard Mean Ocean Water (VSMOW) in per mille (‰), where VSMOW ($D/H_{VSMOW} = 155.76 \times 10^{-6}$) has a δD of 0 by definition, i.e., $\delta D\,(‰) = (\frac{(D/H)_{sample}}{(D/H)_{VSMOW}} - 1) \times 1000$. The δD values reported here are corrected for instrumental mass fractionation (IMF) and for the H-isotopic composition of instrumental background water. Durango and Crystal Lode reference apatites were used to correct IMF for the apatite measurements.

The duration of nakhlite exposure to cosmic rays during their journey to Earth is too short to significantly alter the H and D contents of hydrous phases. Peslier et al. (2019) showed that cosmic ray exposure corrections for nakhlite phases with water contents > 100 µg/g were not significant (D/H on average was 0.3 % lower once corrected). These changes are very minor when compared to the variability between different measurements (even within the same mineral in the same meteorite) and are well within the uncertainty values produced for each measurement. Our measured apatite crystals contain thousands to tens of thousands of µg/g H_2O, hence cosmic ray exposure corrections would result in no change either to the water content or the D/H ratio. For our single augite measurement, the water content (µg/g) would not change, and the D/H ratio would decrease by just 3 ‰, well within the 37 ‰ uncertainty on this measurement.

3 Results

3.1 Apatite texture and composition

SEM imaging revealed that thin-section SM-505, in common with other Lafayette thin-sections, is dominated by elongate clinopyroxene crystals, olivine and orthopyroxene (Fig. 1a). Minor magnetite and areas of mesostasis are present, as well as regions of iddingsite typical of the martian aqueous alteration evident in the nakhlite meteorites. No mineralogical evidence of terrestrial weathering is evident in this thin-section (e.g., calcite or sulphate veins). Thin-section SM-505 contains 22 euhedral-subhedral hexagonal or tabular apatite crystals with a short axis between 20 and 50 µm, as well as numerous smaller crystals. All apatite crystals in this thin-section are associated with areas of mesostasis, commonly surrounded by plagioclase feldspar and/or glass, with titanomagnetite crystals nearby (Fig. 1).

Iddingsite alteration is also associated with a number of the apatite crystals. Despite this association, secondary alteration was not observed within any of these crystals via CL imaging. In fact, all apatite crystals appear homogeneous, with blue luminescence induced by rare earth elements (REE^{3+}) indicating primary igneous crystallisation with no zonation (e.g., Barbarand and Pagel, 2001; Gaft et al., 2015, Fig. 1).

Of the 22 largest apatite crystals within thin-section SM-505, 19 were analysed for mineral chemistry (Table 1). All analysed apatite contains appreciable Si (0.23–0.61 wt% SiO_2) and Fe (0.49–0.96 wt% FeO), in line with previous studies of nakhlite apatite (e.g., McCubbin et al., 2013; Birski et al., 2019; Brounce et al., 2022; Martínez et al., 2023). Also in line with previous studies, Lafayette apatite X-site occupancy shows a wide variation between crystals, covering almost the entire F-Cl-OH range seen within the whole nakhlite group (Fig. 2). Several crystals contain OH proportions towards the upper limit of this range. As OH is calculated on the assumption that F + Cl + OH = 1 it is possible that OH is overestimated if other anions are also occupying the apatite X-site, e.g., O_2, CO_3, S, Br, I (Pan and Fleet, 2002), or if vacancies are present (Martínez et al., 2023). Indeed, for those apatite crystals where hydrogen was measured via SIMS (presented as H_2O abundances in Table 1) there is no correlation between measured H_2O and calculated OH. Apatite 10, for example, has the highest reliably measured H_2O content but not the highest calculated OH proportion. It may therefore be more accurate to state this value as OH/other X-site occupant/vacancy. Despite OH uncertainties, F and Cl abundances are directly measured, hence the wide variation shown in these elements is accurate (Fig. 2).

3.2 Hydrogen isotope ratios

The D/H ratios of eight separate apatite crystals were measured, and range from δD values of −188 to 352 ‰ and H_2O contents of 0.73 to 1.93 wt%, excluding apatite 19 (Table 1, Fig. 3). Apatite 19 shows a considerably higher H_2O content than the other apatite crystals (3.10 wt%), and H hotspots were evident during this analysis indicating

Table 1. Lafayette apatite EMPA and SIMS data.

	Ap 1	Ap 2	Ap 3	Ap 4	Ap 6	Ap 7	Ap 8	Ap 9	Ap 10	Ap 12	Ap 13	Ap 14	Ap 15	Ap 16	Ap 17	Ap 18	Ap 19	Ap 20	Ap 22
P_2O_5	40.39	40.54	40.95	41.28	40.98	40.76	41.18	41.38	40.57	41.57	41.91	41.35	41.41	40.93	40.43	40.06	41.09	40.89	40.85
SiO_2	0.33	0.42	0.26	0.44	0.43	0.61	0.39	0.26	0.23	0.29	0.34	0.52	0.25	0.28	0.39	0.27	0.29	0.35	0.37
TiO_2	0.00	0.00	0.00	0.00	0.00	0.00	0.00	0.00	0.00	0.00	0.00	0.00	0.00	0.00	0.00	0.00	0.00	0.00	0.00
Al_2O_3	0.01	0.03	0.00	0.01	0.03	0.02	0.00	0.01	0.01	0.00	0.02	0.03	0.00	0.01	0.01	0.01	0.01	0.01	0.02
Cr_2O_3	0.00	0.01	0.00	0.00	0.01	0.00	0.01	0.00	0.00	0.00	0.00	0.00	0.00	0.00	0.00	0.00	0.00	0.01	0.00
FeO	0.56	0.46	0.53	0.73	0.86	0.96	0.86	0.53	0.49	0.68	0.76	0.63	0.56	0.89	0.67	0.57	0.62	0.77	0.79
MnO	0.16	0.12	0.15	0.12	0.12	0.14	0.17	0.19	0.19	0.15	0.14	0.11	0.20	0.14	0.12	0.14	0.16	0.15	0.14
MgO	0.02	0.01	0.03	0.02	0.02	0.04	0.05	0.06	0.05	0.04	0.06	0.06	0.04	0.04	0.02	0.04	0.05	0.06	0.04
CaO	53.27	52.82	53.36	53.32	53.21	53.26	54.23	54.07	53.95	54.11	54.33	54.03	53.88	54.06	53.70	53.37	53.76	53.99	53.18
Na_2O	0.08	0.10	0.16	0.14	0.10	0.00	0.05	0.01	0.12	0.04	0.06	0.09	0.10	0.09	0.19	0.03	0.13	0.00	0.07
K_2O	0.01	0.06	0.00	0.01	0.01	0.00	0.00	0.00	0.00	0.00	0.02	0.02	0.00	0.01	0.01	0.00	0.01	0.01	0.02
SO_3	0.00	0.04	0.01	0.00	0.03	0.03	0.01	0.01	0.00	0.04	0.01	0.03	0.01	0.01	0.01	0.01	0.01	0.00	0.01
F	1.53	0.73	1.57	1.21	1.11	1.87	2.10	2.85	1.74	1.31	2.54	2.16	1.73	1.79	1.46	1.86	1.60	2.23	1.96
Cl	2.24	5.49	2.59	3.64	4.19	2.78	2.32	1.24	2.32	4.11	1.56	2.70	1.99	2.41	2.83	2.94	2.76	2.14	2.54
$-O \equiv F$	0.64	0.31	0.66	0.51	0.47	0.79	0.88	1.20	0.73	0.55	1.07	0.91	0.73	0.76	0.61	0.78	0.67	0.94	0.83
$-O \equiv Cl$	0.51	1.24	0.58	0.82	0.95	0.63	0.52	0.28	0.52	0.93	0.35	0.61	0.45	0.54	0.64	0.66	0.62	0.48	0.57
SUM	97.45	99.27	98.35	99.58	99.69	99.04	99.96	99.12	98.40	100.85	100.33	100.21	99.01	99.36	98.59	97.87	99.19	99.18	98.61
Structural formulae based on 13 anions																			
P	2.94	2.95	2.98	3.01	2.99	2.97	3.00	3.01	2.96	3.03	3.05	3.01	3.02	2.98	2.98	2.92	2.99	2.98	2.98
Si	0.03	0.04	0.02	0.04	0.04	0.05	0.03	0.02	0.02	0.02	0.03	0.04	0.02	0.02	0.03	0.02	0.02	0.03	0.03
Al	0.00	0.00	0.00	0.00	0.00	0.00	0.00	0.00	0.00	0.00	0.00	0.00	0.00	0.00	0.00	0.00	0.00	0.00	0.00
Cr	0.00	0.00	0.00	0.00	0.00	0.00	0.00	0.00	0.00	0.00	0.00	0.00	0.00	0.00	0.00	0.00	0.00	0.00	0.00
Ti	0.00	0.00	0.00	0.00	0.00	0.00	0.00	0.00	0.00	0.00	0.00	0.00	0.00	0.00	0.00	0.00	0.00	0.00	0.00
Fe	0.04	0.03	0.04	0.05	0.06	0.07	0.06	0.04	0.04	0.05	0.05	0.05	0.04	0.06	0.05	0.04	0.04	0.06	0.06
Mn	0.02	0.01	0.02	0.01	0.01	0.02	0.02	0.02	0.02	0.02	0.02	0.01	0.02	0.01	0.01	0.02	0.02	0.02	0.02
Mg	0.00	0.00	0.00	0.00	0.00	0.00	0.01	0.01	0.01	0.01	0.01	0.01	0.01	0.01	0.00	0.01	0.01	0.01	0.00
Ca	4.91	4.87	4.92	4.92	4.91	4.91	5.00	4.98	4.97	4.99	5.01	4.98	4.97	4.99	5.00	4.92	4.96	4.98	4.90
Na	0.01	0.02	0.03	0.02	0.02	0.00	0.01	0.00	0.02	0.01	0.01	0.01	0.02	0.02	0.03	0.00	0.02	0.00	0.01
K	0.00	0.01	0.00	0.00	0.00	0.00	0.00	0.00	0.00	0.00	0.00	0.00	0.00	0.00	0.00	0.00	0.00	0.00	0.00
Σ Cations	7.96	7.93	8.01	8.05	8.03	8.02	8.13	8.09	8.03	8.12	8.18	8.12	8.09	8.09	8.11	7.93	8.07	8.07	8.00
F	0.42	0.20	0.43	0.33	0.30	0.51	0.57	0.78	0.47	0.36	0.69	0.59	0.47	0.49	0.40	0.51	0.44	0.61	0.53
Cl	0.33	0.80	0.38	0.53	0.61	0.40	0.34	0.18	0.34	0.60	0.23	0.39	0.29	0.35	0.42	0.43	0.40	0.31	0.37
Σ X-site	0.74	1.00	0.80	0.86	0.91	0.91	0.91	0.96	0.81	0.96	0.92	0.98	0.76	0.84	0.82	0.94	0.84	0.92	0.91
OH*	0.26	0.00	0.20	0.14	0.09	0.09	0.09	0.04	0.19	0.04	0.08	0.02	0.24	0.16	0.18	0.06	0.16	0.08	0.09
SIMS H_2O	0.73		1.17	1.17					1.93				0.97			1.17	3.10		1.44
SUM inc. OH	98.18	99.27	99.52	100.75	99.69	99.04	99.96	99.12	100.33	100.85		100.21	99.98	99.36	98.59	99.04	102.29	99.18	100.05
SIMS δD (‰)	137		206	226					352				148			-188	-179		-2

* OH calculated by assuming $F + Cl + OH = 1$

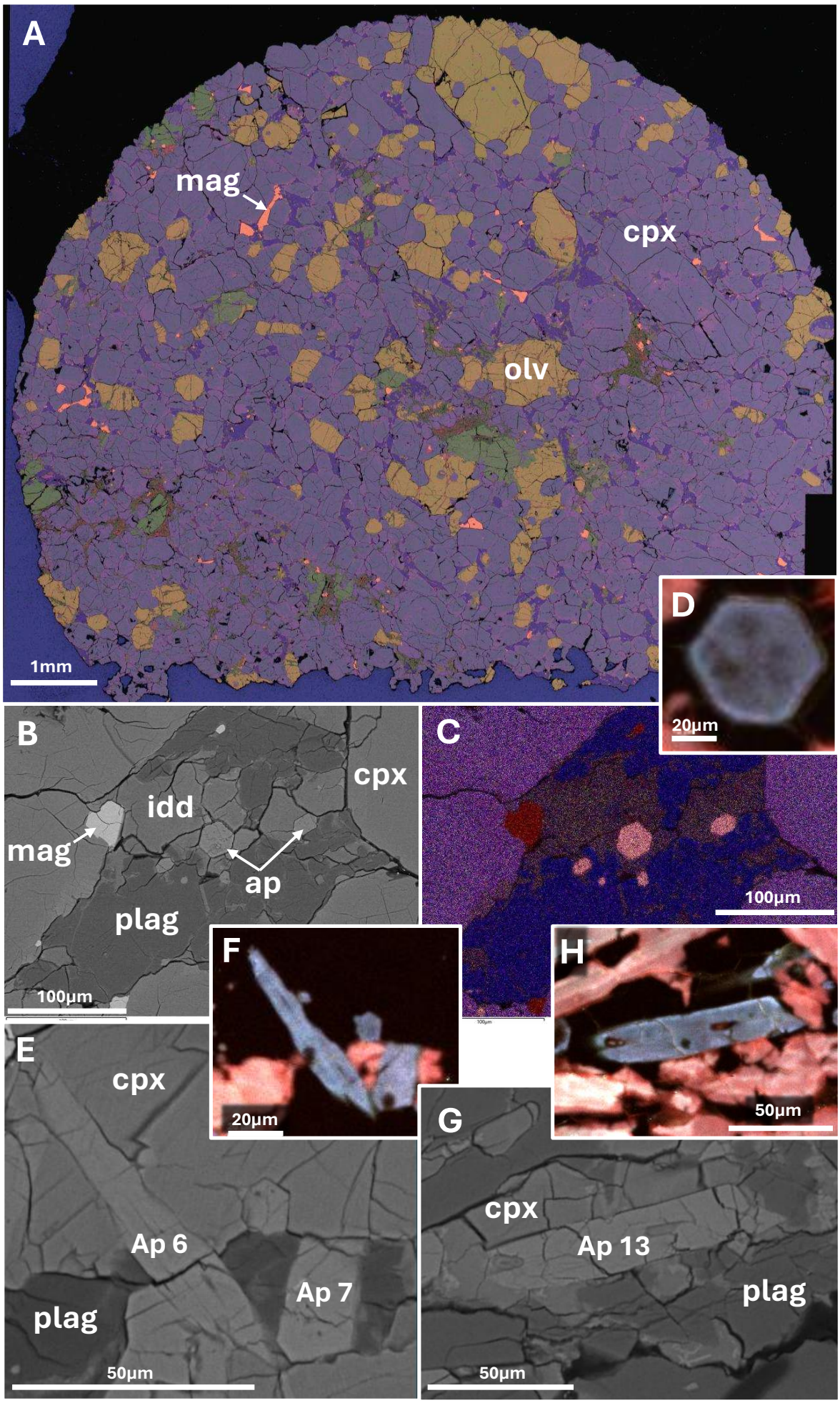
A
mag
cpx
olv
1mm
D
20µm
B
cpx
idd
mag
ap
plag
100µm
C
100µm
F
20µm
H
50µm
E
cpx
Ap 6
Ap 7
plag
50µm
G
cpx
Ap 13
plag
50µm

Figure 1. *(Previous page)* Scanning electron microscope images showing Lafayette thin-section SM-505 and details of its apatite crystals. A) false-colour SEM-EDX image showing the whole thin section, where Fe is red, Mg is green, Si is blue, and Ca is pink. In this image olivine (olv) is shown as yellow, clinopyroxene (cpx) is purple, orthopyroxene is green, magnetite (mag) is orange, and areas of mesostasis (rich in plagioclase) are blue. Brown regions show iddingsite alteration typical of the nakhlite meteorites. Apatite is pink in this image, but crystals are too small to be visible at this scale. B) Backscatter electron image, C) false colour EDX image and D) cathodoluminescence image of apatite 1, where C) has the same colour key as A) with the addition of P = yellow, highlighting apatite grains. These images show apatite 1 is surrounded by iddingsite (idd), but cathodoluminescence images show apatite 1 has not been altered by secondary processes (D). E) Backscatter electron image and F) cathodoluminescence image of apatite 6 and 7 and their associated minerals. G) Backscatter electron image and H) cathodoluminescence image of apatite 13.

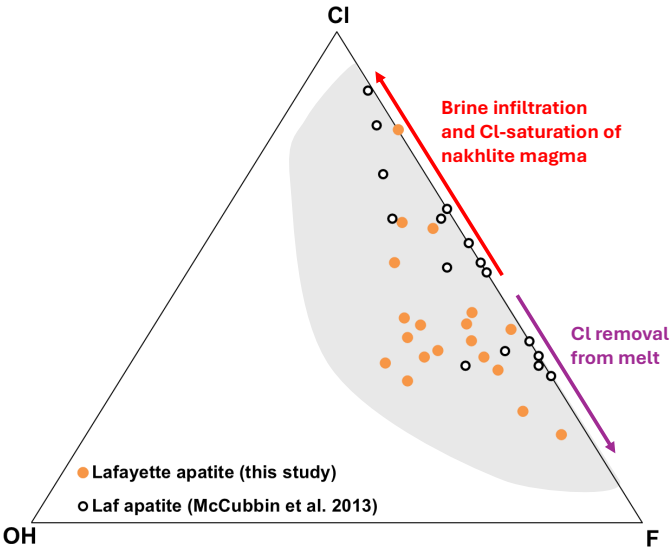

Figure 2. Ternary plot showing the variability in Lafayette apatite X-site occupancy (mol%). Data shown are: this study (orange circles), McCubbin et al. (2013) Lafayette apatite data (open black circles), other nakhlite apatite data (grey envelope encompassing data from McCubbin et al. (2013) and Martínez et al. (2023). Trends of Cl saturation due to brine infiltration to the nakhlite/chassignite cumulate pile, and F enrichment due to Cl removal from the cumulate pile, are shown.

the presence of cracks within this crystal, and BSE images of the resulting analysis pit show that a crack was included at the edge of the apatite grain (see Supplementary Material, Fig. S2, and Hallis et al., 2025). For this reason, data from apatite 19 have been excluded from further discussion.

Of the remaining seven apatite crystals, five contain positive δD values (137 to 352 ‰) and two have negative δD values (−2 and −188 ‰). The analysis pits in these latter two apatite crystals (apatite 18 and 22) do not show any obvious encroachment into cracks or voids, and their water content is within the range of the other analysed apatite crystals. However, the raw data for both analyses show a large decrease in hydrogen counts (both H and D) from cycle 1 to cycle 50, as well as a decrease in the H/O ratio, indicative of surface contamination (see Supplementary Material). If apatite 18 and 22 are excluded from the dataset on suspicion of contamination, the δD range shown by the five remaining apatite crystals is more positive than that reported for Nakhla apatite crystals (δD −78 to 188 ‰; Hallis et al., 2012), and the water contents are higher (Fig. 3). There is a correlation between δD and H_2O content within these five Lafayette apatite crystals, with the most water-rich crystal (apatite 10) showing the highest δD value. This correlation does not extend to F and Cl abundances, where increasing δD shows no correlation with F and Cl abundance (Fig. 3). This Lafayette apatite δD range is similar to that reported for the least degassed augite measured within the nakhlites (Peslier et al., 2019) and Chassigny melt inclusions (Boctor et al., 2003) – although see discussion of chassignite impact shock effects on D/H ratios below. Our single measured augite δD value from Lafayette also fits within this range (195 ± 37 ‰), although because no augite standard materials were measured during SIMS analyses this value has been IMF corrected based on apatite standard values. Our measured Lafayette apatite δD values are similar to the average value for Yamato 980459 melt inclusions (275 ± 20 ‰), which is commonly quoted as the most representative δD value for the shergottite mantle source region (Usui et al., 2012).

4 Discussion

4.1 Apatite in the nakhlites

The Si content of nakhlite apatite crystals could be explained by the presence of a minor amount of the mineral ellestadite, the endmember in the apatite group that contains SiO_4^{4-} and SO_4^{2-} groups substituting for the PO_4^{3-} group. However, ellestadite contains equal parts Si and S, and our EMPA data show that, although S is present, it is not as abundant as Si (Table 1). In addition, ellestadite does not contain Fe, which is more abundant in nakhlite apatite than Si (Table 1; McCubbin et al., 2013; Birski et al., 2019; Brounce et al., 2022; Martínez et al., 2023). Alternatively, both Si and Fe apatite contents could be explained by the ingress of secondary iddingsite alteration into apatite crystals, e.g., along cracks and cleavage planes, but CL images indicate no such alteration (Fig. 1) even where iddingsite is present in the surrounding mesostasis. Transmission electron microscope (TEM) analyses of Nakhla and NWA 998 apatite support this conclusion, showing no evidence of post-magmatic fluid interactions or subsolidus ionic diffusion (Martínez et al., 2023). Importantly, these CL and TEM data show that the post-magmatic aqueous alteration that affected the nakhlites at ≈ 600 Ma did not penetrate into the apatite crystals, hence the D/H ratio of

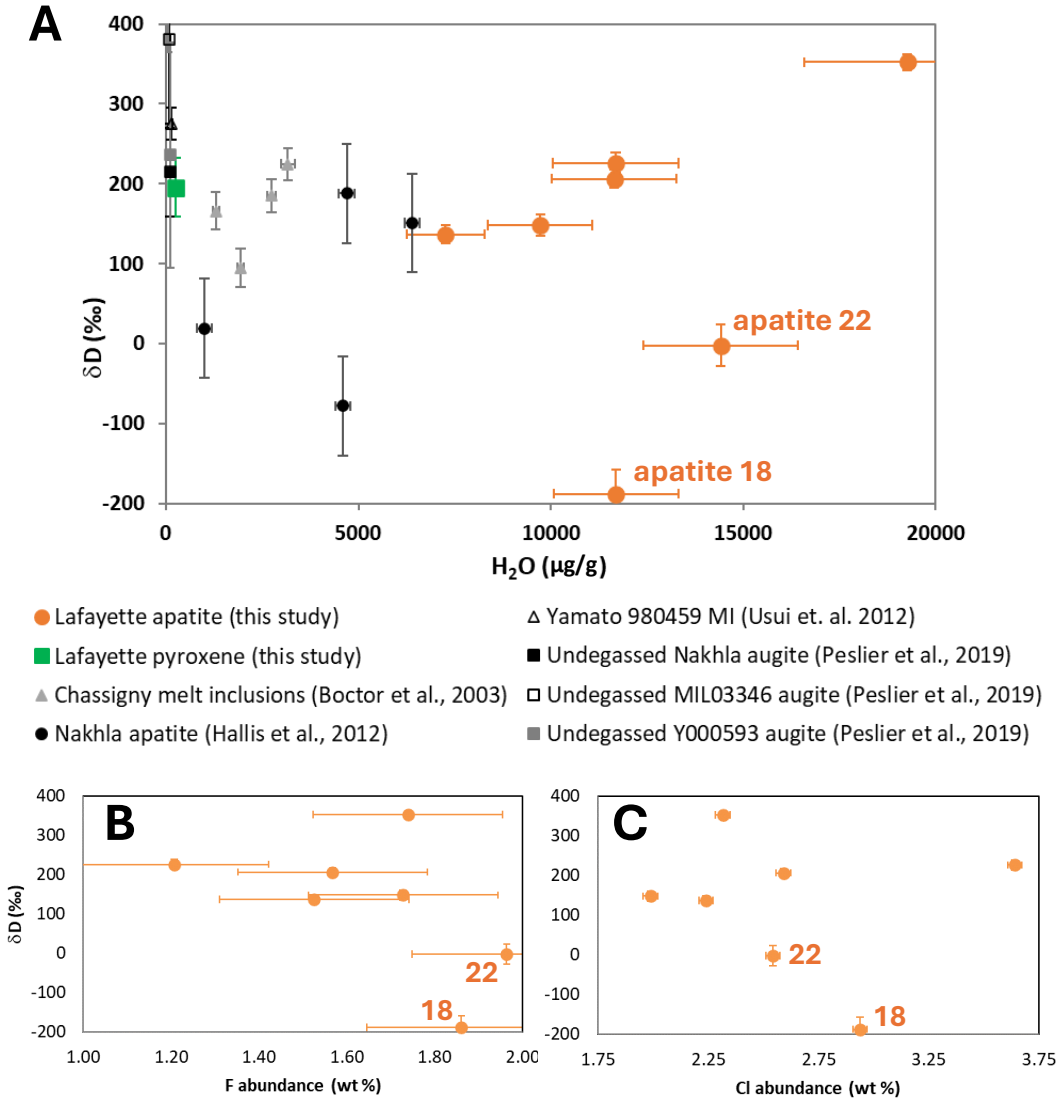

Figure 3. Plots showing D/H ratio (δD, ‰) vs. A) H_2O (µg/g), B) fluorine and C) chlorine abundance (wt%).

these crystals still reflects that of primary magmatic fluid(s). These TEM analyses suggest Nakhla apatite preserves chemical zonation, where Si, Fe, F and REE's are more abundant in the core, and Cl abundance increases towards the rim, consistent with crystallisation from a late-stage and increasingly Cl-rich melt (Martínez et al., 2023). REE zonation is not evident from CL images of the Lafayette apatite crystals analysed in this study, although it is possible that subtle variations are not visible in these relatively low-resolution images (Fig. 1). Cerium variability is evident from previously published Lafayette apatite EMPA data, but this variation is measured between separate crystals rather than zonation within a single crystal (McCubbin et al., 2013).

Variation in Cl, F and (OH/other X-site occupant/vacancy) abundance between grains is evident. The SIMS data do not show a degassing trend (increasing δD with decreasing H_2O abundance; e.g., Tartèse et al., 2014) meaning another process must have caused the X-site occupancy variation. This variation supports incorporation of a Cl-enriched exogenous fluid into the chassignite/nakhlite magma body prior to nakhlite apatite crystallisation (McCubbin et al., 2013). Cl-saturation in the melt resulted in increasing Cl-abundance within apatite, and the following removal of Cl from the melt resulted in crystallisation of more F-rich apatite, hence the wide variation of X-site occupancy in apatite crystals within both Lafayette and Nakhla. The final apatite crystals to crystallise from the nakhlite cumulate pile (e.g., those within the MIL nakhlites) are subsequently Cl-depleted and more F-enriched. Cl isotope ratios for chassignites and nakhlites also support the incorporation of a Cl-rich brine from the crust into the nakhlite melt (Williams et al., 2016; Shearer et al., 2018). Similar interactions have been proposed between terrestrial layered mafic intrusions and Cl-rich fluids (e.g., the Lukkulaisvaara intrusion in northern Karelia, Russia; Glebovitsky et al., 2001).

Martian crustal fluids have the opportunity to equilibrate or partially equilibrate with the extremely elevated D/H ratios of the martian atmosphere if the two come into contact (e.g., Hu et al., 2020). Thus, these fluids would

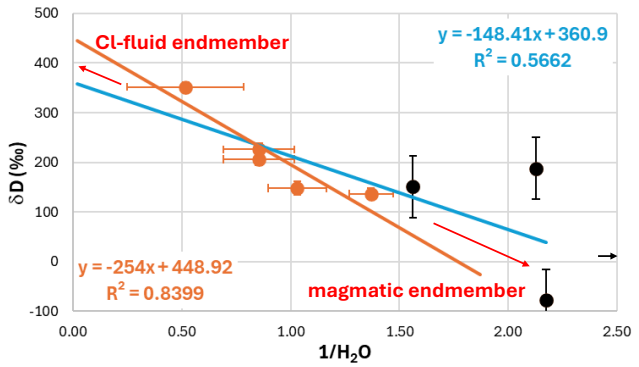

Figure 4. Plot showing D/H ratio (δD, ‰) vs. $1/H_2O$ (wt%), with mixing trends implied by the Lafayette apatite crystals (orange) and the combined Lafayette and Nakhla apatite datasets (blue). The black arrow indicates the position of the fourth Nakhla data point at $1/H_2O = 10$ (1000 µg/g H_2O). The low water content of this apatite crystal in comparison to the others measured in Nakhla and those of Lafayette is anomalous, and when it is included in the trendline calculation the Cl-fluid endmember drops to ~200 ‰. However, the R^2 value of this trendline is 0.2, hence it was decided not to include this fourth Nakhla datapoint in our final trendline calculation.

have elevated D/H ratios compared to those of the martian mantle. The presence of a surficial water/ice component with elevated D/H ratios has been reported in separate shergottite meteorites with differing magmatic origins (Usui et al., 2015). The relatively restricted range of δD values (≈1000–2000 ‰) observed in groundmass glass and impact melt from these shergottites suggests the presence of a common hydrogen reservoir representing hydrated crust and/or ground ice interbedded within sediments. These hydrated crustal reservoirs could have existed globally and relatively intact over geologic time (Usui et al., 2015). However, nakhlite apatite δD values are several hundred per mille lighter (Fig. 3) than the purported hydrated martian crust, possibly indicating the nakhlite-infiltrating Cl-rich brine had never been in contact with the martian atmosphere and thus had D/H ratios similar to those reported for the depleted shergottite mantle (Usui et al., 2012). In support of this scenario (scenario 1) our data show no correlation between increasing apatite Cl-content and increasing D/H ratio (Fig. 3), a trend which should be apparent if the Cl-rich brine had a higher D/H ratio than the nakhlite parental magma. However, our small dataset (5 datapoints) does present limitations in this regard, and a future larger dataset could reveal a trend which is as yet hidden.

Alternatively (scenario 2), it may be the case that nakhlite apatite D/H ratios are the product of mixing between a crustally-derived Cl-rich brine with an intermediate D/H ratio and a mantle source region with a much lower D/H ratio. A plot showing δD vs. 1/(OH) for the five uncontaminated Lafayette apatite measurements (Fig. 4) reveals the possibility of a mixing trend between a D/H ratio magmatic endmember with a negative δD value and a Cl-rich fluid endmember with a D/H ratio at δD ≈ 450 ‰. If the Nakhla apatite dataset is included (Hallis et al., 2012) the resulting trendline indicates a slightly more positive magmatic endmember and a Cl-rich fluid endmember at δD ≈ 350 ‰. In either case, this Cl-rich fluid endmember is still much lighter than the surficial water/ice component measured within the shergottites (1000–2000 ‰; Usui et al., 2015), indicating that the hydrated crust/ground ice at the nakhlite launch site has a lower D/H ratio than that of the shergottite launch site.

Scenario 2 is supported by the high $\delta^{37}Cl$ measured within late stage Chassigny apatite, reportedly produced by a crustal component (the Cl-rich brine) that has interacted with the highly fractionated martian atmosphere (Shearer et al., 2018). In addition, a low D/H ratio for the martian mantle is supported by nitrogen isotope ($^{15}N/^{14}N$) ratios, indicating an isotopically light martian mantle (Mathew and Marti, 2001; Mohapatra and Murty, 2003). As hydrogen and nitrogen isotope ratios are positively correlated in extraterrestrial materials (e.g., Marty, 2012), a low $^{15}N/^{14}N$ ratio for the martian mantle suggests a low D/H ratio. Scenario 2 would imply the D/H ratios measured within the least degassed nakhlite augite crystals (δD 430 ± 172 ‰; Peslier et al., 2019) reflect the D/H ratio of the Cl-rich brine. Although it is clear that more volatile isotope data is required from the nakhlites and other martian lithologies before either scenario can be proved, we believe the weight of evidence is currently in favour of scenario 2.

4.2 The D/H ratio of the martian mantle

Our Lafayette apatite data, along with apatite data from Nakhla (Hallis et al., 2012), melt inclusion data from Chassigny (Boctor et al., 2003), and data from the least degassed nakhlite augite crystals (Peslier et al., 2019), all converge on a D/H ratio range of δD −78 to 430 ‰. Thus, regardless of which of the two above scenarios are correct, this D/H range sits between terrestrial upper mantle values (e.g., Deloule et al., 1991) and an upper limit slightly higher than the D/H ratio measured in glassy melt inclusions within shergottite Y980459 (δD 275 ‰; Usui et al., 2012), reportedly reflecting the depleted shergottite mantle source region. The similarity between D/H ratios within the nakhlite/chassignite and depleted shergottite mantle source regions could suggest global homogeneity for the martian mantle. However, little is known about how early martian volcanic degassing and atmospheric production affected the D/H ratio of the martian mantle, so it is unclear whether the mantle signatures measured in these meteorites represent the primordial martian mantle. Based on the volume of volcanic material identified at the surface, and on the derived abundance of water in the mantle, Jakosky and Treiman (2023) reported that volcanic outgassing supplied no more than ≈10% of the current martian surface H_2O inventory. This calculation is based on the current martian geologic record, hence cannot take into account any degassing before the late Noachian period because much of the geologic record does not survive prior to this (e.g., Jakosky and Hallis, 2024). In general, volcanic degassing would increase

the D/H ratio within the residual mantle, but the extent of this increase can only be calculated if the amount of degassing is known. The enriched shergottites contain extremely high D/H ratios, and it has been argued that they represent a separate mantle source region to the depleted shergottites and chassignites/nakhlites, with a much higher D/H ratio ($\delta D \approx 4000$ ‰; Barnes et al., 2020), indicative of a heterogeneous martian mantle with respect to D/H ratio. It is possible that these high D/H ratios represent a heavily degassed source region within the mantle, or increased interactions with the atmosphere due to an impact event at this site. Further volatile isotope measurements of these meteorites would help clarify the existing D/H datasets.

The nakhlites and chassignites are known to be launch paired, with both meteorite types having originated from the same site on Mars. However, the average shock pressures recorded in the chassignites (≥ 35 GPa; e.g., Langenhorst and Greshake, 1999) are much higher than those recorded in the nakhlites (< 15 GPa; e.g., Treiman, 2005; Daly et al., 2019a) and this has had an effect on D/H ratios of hydrous phases within the chassignites. Giesting et al. (2015) explain that the high D/H ratios measured in the amphibole of chassignite NWA 2737 ($\delta D \approx 3700$ ‰) are due to intense shock-induced degassing of the lighter H isotope. The D/H ratio of a single apatite crystal in Chassigny was reported by Boctor et al. (2003), $D/H = 811 \pm 23$ ‰, $H_2O = 2130 \pm 90$ µg/g. This value is closer to the Lafayette apatite values measured during this study, and the level of shock evidenced within Chassigny is less than NWA 2737 (35 GPa vs. 55 GPa; Langenhorst and Greshake, 1999; Giesting et al., 2015, and references therein). Nevertheless, 35 GPa is a significant level of shock, hence the D/H ratios measured in Chassingy's hydrous phases (apatite, amphibole and melt inclusions) may still have been elevated by shock induced degassing. Thus, the Chassigny melt inclusion D/H ratios included in Figure 3a may have been lower when this meteorite originally crystallised.

Based on the data presented above we can conclude that Mars' primordial mantle had a D/H ratio of $\delta D < 430$ ‰, and if scenarior 2 is correct this value could be less than −100 ‰. A low martian mantle D/H ratio could support carbonaceous (C-)chondrite delivery of water to Mars during the planet's formation (e.g., Alexander et al., 2012; Alexander, 2017). Chondritic delivery of volatile elements to Mars is in agreement with nitrogen isotope measurements of melt inclusions within Chassigny and several nakhlites (Deligny et al., 2023). A similar D/H ratio for the martian and terrestrial mantles is also consistent with the small range in D/H ratios observed in nominally anhydrous minerals collected from the asteroid Itokawa (Jin and Bose, 2019) and in enstatite (E-)chondrite meteorites (Piani et al., 2020). Lower D/H ratios have been reported in other inner Solar System materials, for example the mantle source reservoir of the eucrites from protoplanet 4 Vesta (δD -373 ± 127 ‰; Stephant et al., 2021), the angrite parent body (δD -235 ± 113 ‰; Rider-Stokes et al., 2024), the matrix of unequilibrated ordinary chondrites (δD −320 to −71 ‰; Grant et al., 2024), and nominally anhydrous minerals in acapulcoites and lodranites (δD -211 ± 145 ‰; Stephant et al., 2023). These low D/H ratios could have been produced by the accretion of water ice isotopically similar to that accreted by C-chondrites or fractionated nebula water (Grant et al., 2024; Rider-Stokes et al., 2024), rather than bulk-rock C-chondrites. This heterogeneity between the D/H ratios of different bodies within the inner Solar System may thus reflect differing water sources, or differing proportional contributions from multiple water sources.

5 Conclusions

Our Lafayette data support the incorporation of a Cl-rich exogenous fluid into the chassignite/nakhlite magma body prior to nakhlite apatite crystallisation. We propose that this Cl-rich fluid had a D/H ratio lower ($\delta D \approx 400$ ‰) than the hydrated crustal component within the shergottite meteorites. Our Lafayette apatite D/H data, along with similar data from other nakhlite and chassignite hydrous phases, converge on a range between δD −78 and 430 ‰. We propose that the lower end of this range is representative of the martian mantle, supporting carbonaceous chondrite delivery of water to Mars during planetary accretion.

Ultimately, martian meteorites provide a snapshot in time and place on Mars, and gaining a global picture from these limited lithologies is difficult. In this regard, returned samples from Jezero crater could provide key information about the D/H ratio of the mantle, crust and atmosphere at different times and in a different place to any recorded by the current meteorite collection.

Acknowledgements

We thank the Smithsonian Natural History Museum for the Lafayette sample loan. We thank Dr. Liene Spruzeniece at the University of Glasgow GEMS facility, Dr. Tobias Salge at the Natural History Museum London, and Dr. Chris Hayward at the University of Edinburgh for their help with SEM and EMP data collection. Thanks are given to two anonymous reviewers, who helped improve and expand this manuscript. This research was funded via the Leverhulme Trust Research Grant RPG-2018-298 and by a University of Glasgow Rewarding Excellence grant.

Data, code, and outputs availability

The data that support the findings of this study and the sample localities are available from Hallis et al. (2025) at http://doi.org/10.60520/IEDA/113748. Supplementary Material and main text figures and table are available for download in the online version of this article.

Competing interests

The authors declare no competing interests.

Licence agreement

References

Alexander CMO (2017). The origin of inner Solar System water. *Philosophical Transactions of the Royal Society A: Mathematical, Physical and Engineering Sciences* 375(2094): 20150384. doi:10.1098/rsta.2015.0384.

Alexander CMO, Bowden R, Fogel ML, Howard KT, Herd CDK, Nittler LR (2012). The Provenances of Asteroids, and Their Contributions to the Volatile Inventories of the Terrestrial Planets. *Science* 337(6095): 721–723. doi:10.1126/science.1223474.

Barbarand J, Pagel M (2001). Cathodoluminescence study of apatite crystals. *American Mineralogist* 86(4): 473–484. doi:10.2138/am-2001-0411.

Barnes J, Franchi I, Anand M, Tartèse R, Starkey N, Koike M, Sano Y, Russell S (2013). Accurate and precise measurements of the D/H ratio and hydroxyl content in lunar apatites using NanoSIMS. *Chemical Geology* 337: 48–55. doi:10.1016/j.chemgeo.2012.11.015.

Barnes JJ, McCubbin FM, Santos AR, Day JM, Boyce JW, Schwenzer SP, Ott U, Franchi IA, Messenger S, Anand M, others (2020). Multiple early-formed water reservoirs in the interior of Mars. *Nature Geoscience* 13(4): 260–264. doi:10.1038/s41561-020-0552-y.

Birski L, Słaby E, Chatzitheodoridis E, Wirth R, Majzner K, Kozub-Budzyń GA, Sláma J, Liszewska K, Kocjan I, Zagórska A (2019). Apatite from NWA 10153 and NWA 10645—The key to deciphering magmatic and fluid evolution history in nakhlites. *Minerals* 9(11): 695. doi:10.3390/min9110695.

Boctor N, Alexander CO, Wang J, Hauri E (2003). The sources of water in Martian meteorites: Clues from hydrogen isotopes. *Geochimica et Cosmochimica Acta* 67(20): 3971–3989. doi:10.1016/S0016-7037(03)00234-5.

Brounce M, Boyce JW, McCubbin FM (2022). Sulfur in apatite from the Nakhla meteorite record a late-stage oxidation event. *Earth and Planetary Science Letters* 595: 117784. doi:10.1016/j.epsl.2022.117784.

Cohen BE, Mark DF, Cassata WS, Lee MR, Tomkinson T, Smith CL (2017). Taking the pulse of Mars via dating of a plume-fed volcano. *Nature Communications* 8(1): 640. doi:10.1038/s41467-017-00513-8.

Corrigan CM, Velbel MA, Vicenzi EP (2015). Modal abundances of pyroxene, olivine, and mesostasis in nakhlites: Heterogeneity, variation, and implications for nakhlite emplacement. *Meteoritics & Planetary Science* 50(9): 1497–1511. doi:10.1111/maps.12492.

Daly L, Lee MR, Piazolo S, Griffin S, Bazargan M, Campanale F, Chung P, Cohen BE, Pickersgill A, Hallis LJ, others (2019a). Boom boom pow: Shock-facilitated aqueous alteration and evidence for two shock events in the Martian nakhlite meteorites. *Science Advances* 5(9): eaaw5549. doi:10.1126/sciadv.aaw5549.

Daly L, Piazolo S, Lee MR, Griffin S, Chung P, Campanale F, Cohen BE, Hallis LJ, Trimby PW, Baumgartner R, others (2019b). Understanding the emplacement of Martian volcanic rocks using petrofabrics of the nakhlite meteorites. *Earth and Planetary Science Letters* 520: 220–230. doi:10.1016/j.epsl.2019.05.050.

Davidson J, Wadhwa M, Hervig RL, Stephant A (2020). Water on Mars: Insights from apatite in regolith breccia Northwest Africa 7034. *Earth and Planetary Science Letters* 552: 116597. doi:10.1016/j.epsl.2020.116597.

Day JM, Taylor LA, Floss C, Mcsween Jr HY (2006). Petrology and chemistry of MIL 03346 and its significance in understanding the petrogenesis of nakhlites on Mars. *Meteoritics & Planetary Science* 41(4): 581–606. doi:10.1111/j.1945-5100.2006.tb00484.x.

Deligny C, Füri E, Deloule E, Peslier A, Faure F, Marrocchi Y (2023). Origin of nitrogen on Mars: First in situ N isotope analyses of martian meteorites. *Geochimica et Cosmochimica Acta* 344: 134–145. doi:10.1016/j.gca.2023.01.017.

Deloule E, Albarede F, Sheppard SM (1991). Hydrogen isotope heterogeneities in the mantle from ion probe analysis of amphiboles from ultramafic rocks. *Earth and Planetary Science Letters* 105(4): 543–553. doi:10.1016/0012-821X(91)90191-J.

Dong C, Lee Y, Ma Y, Lingam M, Bougher S, Luhmann J, Curry S, Toth G, Nagy A, Tenishev V, others (2018). Modeling Martian atmospheric losses over time: Implications for exoplanetary climate evolution and habitability. *The Astrophysical Journal Letters* 859(1): L14. doi:10.3847/2041-8213/aac489.

Gaft M, Reisfeld R, Panczer G (2015). *Modern luminescence spectroscopy of minerals and materials*. Springer. doi:10.1007/978-3-319-24765-6.

Giesting PA, Schwenzer SP, Filiberto J, Starkey NA, Franchi IA, Treiman AH, Tindle AG, Grady MM (2015). Igneous and shock processes affecting chassignite amphibole evaluated using chlorine/water partitioning and hydrogen isotopes. *Meteoritics & Planetary Science* 50(3): 433–460. doi:10.1111/maps.12430.

Glebovitsky VA, Semenov VS, Belyatsky BV, Koptev-Dvornikov EV, Pchelintseva NF, Kireev BS, Koltsov AB (2001). The structure of the Lukkulaisvaara intrusion, Oulanka group, northern Karelia: petrological implications. *The Canadian Mineralogist* 39(2): 607–637. doi:10.2113/gscanmin.39.2.607.

Grant H, Tartèse R, Jones R, Piani L, Marrocchi Y (2024). Identification of a primordial high D/H component in the matrix of unequilibrated ordinary chondrites. *Geochimica et Cosmochimica Acta* 378: 58–70. doi:10.1016/j.gca.2024.06.005.

Hallis L, Christou E, Davidson J, Distel A, Hervig R (2025). Lafayette martian meteorite SIMS (D/H ratio) and EMPA data from apatite mineral grains, Version 1.0. Interdisciplinary Earth Data Alliance (IEDA). doi:10.60520/IEDA/113748.

Hallis L, Taylor G, Nagashima K, Huss G (2012). Magmatic water in the martian meteorite Nakhla. *Earth and Planetary Science Letters* 359: 84–92. doi:10.1016/j.epsl.2012.09.049.

Harries D, Zhao X, Franchi I (2023). Upper limits of water contents in olivine and orthopyroxene of equilibrated chondrites and several achondrites. *Meteoritics & Planetary Science* 58(5): 705–721. doi:10.1111/maps.13980.

Hu S, Lin Y, Anand M, Franchi I, Zhao X, Zhang J, Hao J, Zhang T, Yang W, Changela H (2020). Deuterium and 37chlorine rich fluids on the surface of Mars: Evidence from the enriched basaltic shergottite Northwest Africa 8657. *Journal of Geophysical Research: Planets* 125(9): e2020JE006537. doi:10.1029/2020JE006537.

Jakosky BM, Brain D, Chaffin M, Curry S, Deighan J, Grebowsky J, Halekas J, Leblanc F, Lillis R, Luhmann JG, others (2018). Loss of the Martian atmosphere to space: Present-day loss rates determined from MAVEN observations and integrated loss through time. *Icarus* 315: 146–157. doi:10.1016/j.icarus.2018.05.030.

Jakosky BM, Hallis LJ (2024). Fate of an earth-like water inventory on Mars. *Journal of Geophysical Research: Planets* 129(2): e2023JE008159. doi:10.1029/2023JE008159.

Jakosky BM, Treiman AH (2023). Mars volatile inventory and outgassing history. *Icarus* 402: 115627. doi:10.1016/j.icarus.2023.115627.

Jin Z, Bose M (2019). New clues to ancient water on Itokawa. *Science Advances* 5(5): eaav8106. doi:10.1126/sciadv.aav8106.

Langenhorst F, Greshake A (1999). A transmission electron microscope study of Chassigny: Evidence for strong shock metamorphism. *Meteoritics & Planetary Science* 34(1): 43–48. doi:10.1111/j.1945-5100.1999.tb01730.x.

Lentz RF, Taylor G, Treiman A (1999). Formation of a martian pyroxenite: A comparative study of the nakhlite meteorites and Theo's Flow. *Meteoritics & Planetary Science* 34(6): 919–932. doi:10.1111/j.1945-5100.1999.tb01410.x.

Marty B (2012). The origins and concentrations of water, carbon, nitrogen and noble gases on Earth. *Earth and Planetary Science Letters* 313: 56–66. doi:10.1016/j.epsl.2011.10.040.

Martínez M, Shearer CK, Brearley AJ (2023). Nanostructural domains in martian apatites that record primary subsolidus exsolution of halogens: Insights into nakhlite petrogenesis. *American Mineralogist* 108(11): 2024–2042. doi:10.2138/am-2022-8794.

Mathew K, Marti K (2001). Early evolution of Martian volatiles: Nitrogen and noble gas components in ALH84001 and Chassigny. *Journal of Geophysical Research: Planets* 106(E1): 1401–1422. doi:10.1029/2000JE001255.

McCubbin FM, Elardo SM, Shearer Jr CK, Smirnov A, Hauri EH, Draper DS (2013). A petrogenetic model for the comagmatic origin of chassignites and nakhlites: Inferences from chlorine-rich minerals, petrology, and geochemistry. *Meteoritics & Planetary Science* 48(5): 819–853. doi:10.1111/maps.12095.

McCubbin FM, Nekvasil H (2008). Maskelynite-hosted apatite in the Chassigny meteorite: Insights into late-stage magmatic volatile evolution in martian magmas. *American Mineralogist* 93(4): 676–684. doi:10.2138/am.2008.2558.

Misawa K, Shih CY, Wiesmann H, Garrison DH, Nyquist LE, Bogard DD (2005). Rb-Sr, Sm-Nd and Ar-Ar isotopic systematics of Antarctic nakhlite Yamato 000593. *Antarctic meteorite research* 18: 133–151. doi:10.15094/00006069.

Mohapatra RK, Murty S (2003). Precursors of Mars: Constraints from nitrogen and oxygen isotopic compositions of martian meteorites. *Meteoritics & Planetary Science* 38(2): 225–241. doi:10.1111/j.1945-5100.2003.tb00261.x.

Mosenfelder JL, Le Voyer M, Rossman GR, Guan Y, Bell DR, Asimow PD, Eiler JM (2011). Analysis of hydrogen in olivine by SIMS: Evaluation of standards and protocol. *American Mineralogist* 96(11-12): 1725–1741. doi:10.2138/am.2011.3810.

Nyquist L, Bogard D, Shih CY, Greshake A, Stöffler D, Eugster O (2001). Ages and geologic histories of Martian meteorites. *Space Science Reviews* 96(1): 105–164. doi:10.1023/A:1011993105172.

O'Brien AC, Hallis LJ, Regnault C, Morrison D, Blackburn G, Steele A, Daly L, Tait A, Tremblay MM, Telenko DE, others (2022). Using Organic Contaminants to Constrain the Terrestrial Journey of the Martian Meteorite Lafayette. *Astrobiology* 22(11): 1351–1362.

Okazaki R, Nagao K, Imae N, Kojima H (2003). Noble gas signatures of Antarctic nakhlites, Yamato (Y) 000593, Y000749, and Y000802. *Antarctic meteorite research* 16: 58–79. doi:10.15094/00006026.

Pan Y, Fleet ME (2002). Compositions of the apatite-group minerals: substitution mechanisms and controlling factors. *Reviews in mineralogy and geochemistry* 48(1): 13–49. doi:10.2138/rmg.2002.48.2.

Peslier A, Hervig R, Yang S, Humayun M, Barnes J, Irving A, Brandon A (2019). Determination of the water content and D/H ratio of the martian mantle by unraveling degassing and crystallization effects in nakhlites. *Geochimica et Cosmochimica Acta* 266: 382–415. doi:10.1016/j.gca.2019.04.023.

Piani L, Marrocchi Y, Rigaudier T, Vacher LG, Thomassin D, Marty B (2020). Earth's water may have been inherited from material similar to enstatite chondrite meteorites. *Science* 369(6507): 1110–1113. doi:10.1126/science.aba1948.

Rider-Stokes B, Stephant A, Anand M, Franchi I, Zhao X, White L, Yamaguchi A, Greenwood R, Jackson S (2024). Evidence against water delivery by impacts within 10 million years of planetesimal formation. *Earth and Planetary Science Letters* 642: 118860. doi:10.1016/j.epsl.2024.118860.

Shearer C, Messenger S, Sharp Z, Burger P, Nguyen A, McCubbin F (2018). Distinct chlorine isotopic reservoirs on Mars. Implications for character, extent and relative timing of crustal interactions with mantle-derived magmas, evolution of the martian atmosphere, and the building blocks of an early Mars. *Geochimica et Cosmochimica Acta* 234: 24–36. doi:10.1016/j.gca.2018.04.034.

Stephant A, Wadhwa M, Hervig R, Bose M, Zhao X, Barrett T, Anand M, Franchi I (2021). A deuterium-poor water reservoir in the asteroid 4 Vesta and the inner solar system. *Geochimica et Cosmochimica Acta* 297: 203–219. doi:10.1016/j.gca.2021.01.004.

Stephant A, Zhao X, Anand M, Davidson J, Carli C, Cuppone T, Pratesi G, Franchi I (2023). Hydrogen in acapulcoites and lodranites: A unique source of water for planetesimals in the inner Solar System. *Earth and Planetary Science Letters* 615: 118202. doi:10.1016/j.epsl.2023.118202.

Tartèse R, Anand M, McCubbin FM, Elardo SM, Shearer CK, Franchi IA (2014). Apatites in lunar KREEP basalts: The missing link to understanding the H isotope systematics of the Moon. *Geology* 42(4): 363–366. doi:10.1130/G35288.1.

Treiman AH (2005). The nakhlite meteorites: Augite-rich igneous rocks from Mars. *Geochemistry* 65(3): 203–270. doi:10.1016/j.chemer.2005.01.004.

Udry A, Day JM (2018). 1.34 billion-year-old magmatism on Mars evaluated from the co-genetic nakhlite and chassignite meteorites. *Geochimica et Cosmochimica Acta* 238: 292–315. doi:10.1016/j.gca.2018.07.006.

Udry A, Howarth GH, Herd CDK, Day JMD, Lapen TJ, Filiberto J (2020). What Martian Meteorites Reveal About the Interior and Surface of Mars. *Journal of Geophysical Research: Planets* 125(12): e2020JE006523. doi:10.1029/2020JE006523.

Udry A, Ostwald AM, Day JM, Hallis LJ (2025). Fundamental constraints and questions from the study of martian meteorites and the need for returned samples. *Proceedings of the National Academy of Sciences* 122(2): e2404254121. doi:10.1073/pnas.2404254121.

Usui T, Alexander CM, Wang J, Simon JI, Jones JH (2012). Origin of water and mantle–crust interactions on Mars inferred from hydrogen isotopes and volatile element abundances of olivine-hosted melt inclusions of primitive shergottites. *Earth and Planetary Science Letters* 357: 119–129. doi:10.1016/j.epsl.2012.09.008.

Usui T, Alexander CM, Wang J, Simon JI, Jones JH (2015). Meteoritic evidence for a previously unrecognized hydrogen reservoir on Mars. *Earth and Planetary Science Letters* 410: 140–151. doi:10.1016/j.epsl.2014.11.022.

Villanueva G, Mumma M, Novak R, Käufl H, Hartogh P, Encrenaz T, Tokunaga A, Khayat A, Smith M (2015). Strong water isotopic anomalies in the martian atmosphere: Probing current and ancient reservoirs. *Science* 348(6231): 218–221. doi:10.1126/science.aaa3630.

Webster CR, Mahaffy PR, Flesch GJ, Niles PB, Jones JH, Leshin LA, Atreya SK, Stern JC, Christensen LE, Owen T, others (2013). Isotope ratios of H, C, and O in CO2 and H2O of the Martian atmosphere. *Science* 341(6143): 260–263. doi:10.1126/science.1237961.

Williams J, Shearer C, Sharp Z, Burger P, McCubbin F, Santos A, Agee C, McKeegan K (2016). The chlorine isotopic composition of Martian meteorites 1: Chlorine isotope composition of Martian mantle and crustal reservoirs and their interactions. *Meteoritics & Planetary Science* 51(11): 2092–2110. doi:10.1111/maps.12647.